Uncertainty Analysis of an Interfacial Area Reconstruction Algorithm

A. Dave, A. Manera
Department of Nuclear Engineering and Radiological Sciences
University of Michigan
Ann Arbor, MI 48105, USA
akshayjd@umich.edu

M. Beyer, D. Lucas
Helmholtz-Zentrum Dresden-Rossendorf
Institute of Fluid Dynamics
01314 Dresden, Germany

H.-M. Prasser
Department of Mechanical and Process Engineering
ETH Zurich
8092 Zurich, Switzerland

ABSTRACT

Wire mesh sensors (WMS) are state of the art devices that allow high resolution (in space and time) measurement of 2D void fraction distribution in any two-phase flow regime. Data using WMS have been recorded at the Helmholtz Zentrum Dresden Rossendorf (HZDR) [1] for a wide combination of superficial gas and liquid velocities, providing an excellent database for advances in two-phase flow modeling. In two-phase flow, the interfacial area plays an integral role in coupling the mass, momentum and energy transport equations of the liquid and gas phase. While current models used in best-estimate thermal-hydraulic codes (e.g. RELAP5, TRACE, TRACG, etc.) are still based on algebraic correlations for the estimation of the interfacial area in different flow regimes, interfacial area transport equations (IATE) have been proposed to predict the dynamic propagation in space and time of interfacial area [2]. IATE models are still under development and the HZDR WMS experiments would provide an excellent basis for the validation and further advance of these models. The current paper is focused on the algorithms used to reconstruct interfacial area densities from the void-fraction voxel data measured using WMS.

In previous research efforts, a surface triangularization algorithm has been developed in order to estimate the surface area of individual bubbles recorded with the WMS, and estimate the interfacial area in the given flow condition. In the present paper, synthetically generated bubbles are used to assess the algorithm's accuracy. As the interfacial area of the synthetic bubbles are defined by user inputs, the error introduced by the algorithm can be quantitatively obtained.

In the present paper, the accuracy of interfacial area measurements is characterized for different bubbles sizes and shapes, and for different WMS acquisition frequencies. It is found that while convex shapes are successfully analyzed by the reconstruction algorithm, difficulties are faced when concave shapes such as internal cavities are introduced.

KEYWORDS
Wire mesh sensor, two-phase flow, interfacial area transport equation, uncertainty analysis

1. INTRODUCTION

In the past several years, numerous models have been developed for two phase flows. Generally, they vary complexity, in number of transport equations required and closure relationships needed. Generally, greater accuracy is achieved at the cost of complexity. Depending on the flow being modeled, it is at times unnecessary to employ complex models.

The most popular models used in nuclear engineering safety analyses are based on the two-fluid formulation, where separate mass, momentum and energy balance equations are formulated for the gas and liquid phase respectively, resulting in six transport equations. The six-equation two-fluid model is most appropriate for transients where flow conditions are rapidly changing and non-equilibrium between the phases exists. For example, the time lag of energy transfer at the interface between liquid and gas may cause temperature differences between the gas and liquid phase. In the six-equation two-fluid formulation, several closure relationships are needed in order to model the interfacial transfer terms which couple the transport equations of the two phases. As described by Ishii and Kim [3], these terms can be expressed by Eq. (1),

$$(Interfacial\ Transfer\ Term) \propto a_i \cdot (Driving\ Force) \tag{1}$$

where a_i represents the interfacial area concentration (surface area per unit volume). As the interfacial transfer terms couple the two phases, the importance of being able to correctly predict the interfacial area concentration is apparent. Since the time one-group and two-group interfacial area transport equation (IATE) have been introduced by Ishii and Kim [3], several experimental efforts have focused on IATE models validation.

Detailed measurements of two-phase flows is a challenging task. Recent validation efforts by Talley [4], Bernard et al. [5], and Smith et al. [6] have used experimental data from conductivity probes, which are able to measure the local time-averaged void fraction by ensemble of phase indicator data recorded at about 10-30 kHz.

The wire mesh sensor, pioneered by Prasser et al. [7], is also an intrusive device used to measure void fractions in two-phase flows. In contrast to the conductivity probe however, the wire mesh sensor is able to measure void fractions simultaneously at multiple locations in a pipe cross section, resulting in a time-dependent 2D void-fraction distribution. A typical wire mesh sensor features a spatial resolution of 3 mm and can provide up to 10,000 frames/s.

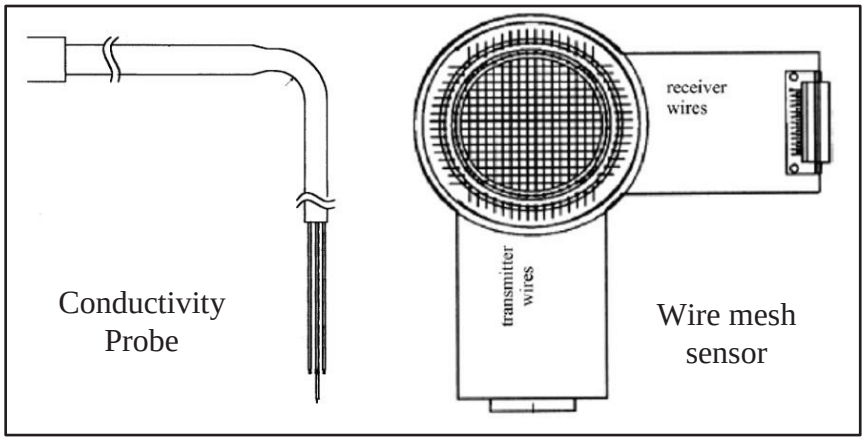

Figure 1: Physical comparison of the conductivity probe [8] and the wire mesh sensor [9].

The capability of providing time dependent 2D void fraction distributions and the potential for a complete 3D surface reconstruction of the two-phase flow interface (see an example in Figure 2 for a churn-turbulent flow regime) is one of the biggest advantages of the wire mesh sensors over needle probes [9]. In addition, the very short time (about 10 s) required to perform a complete measurement at a given operational condition has allowed HZDR to cover a very wide range of operational conditions in a relatively short period of time [10].

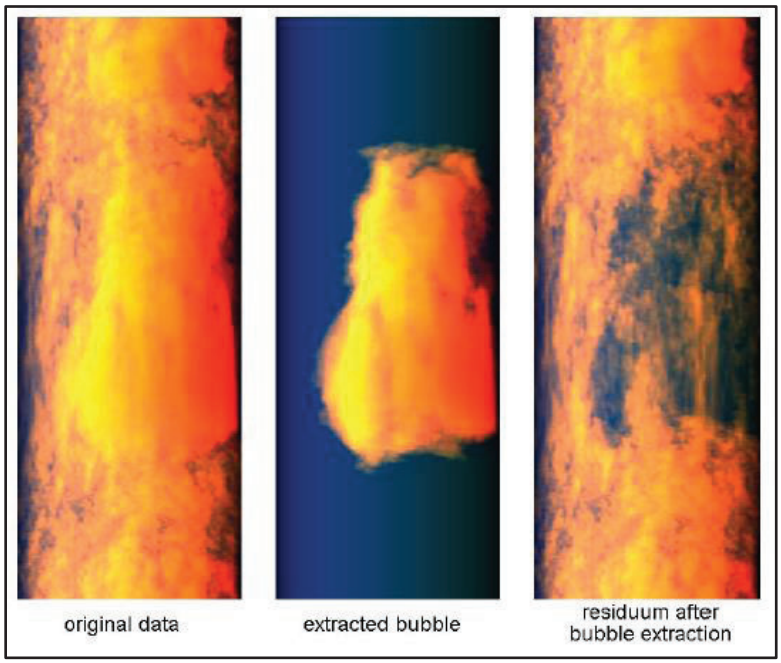

Figure 2: A single bubble structure is subtracted from a churn-turbulent flow; the data has been acquired by a wire mesh sensor [9].

Both needle probes and WMS require post-processing in order to estimate the interfacial area concentration. The focus of this paper is on the uncertainty analysis of the post-processing algorithm (hereafter referred to as 'HZD algorithm') that has been initially developed by Prasser [11] and later on extended by Beyer and Lucas [10]. For a meaningful validation of the IATE model, any error introduced by the HZD algorithm in the estimation of the experimental interfacial area density needs to be quantified.

The approach presented in this paper attempts to quantify the error on the interfacial area by synthetically generating bubbles. For a given set of bubbles defined by the user and moving through the pipe cross-section at a user-defined velocity, we first generate a WMS "data file" as it would be measured by an ideal WMS placed in that user-defined two-phase flow. The shape, location in the pipe cross-section, and velocity of the bubble are inputs. Furthermore, the frequency at which the synthetic bubbles are recorded can also be modified (allowing analysis of appropriate wire mesh sensor operating frequencies). The following section will provide a high level description of the HZD algorithm used to reconstruct interfacial area.

2. INTERFACIAL AREA RECONSTRUCTION ALGORITHM

The raw data produced by wire mesh sensors consists of local conductivity measurements that is two-dimensional in space and acquired at a set frequency. As illustrated in Figure 3, the wire mesh sensor

measures an average fluid conductivity across a square about each grid point. The data is therefore a collection of voxels. By using calibration data for liquid and gas conductivity and assuming a linear dependence of the flow conductivity with respect to the local void fraction, the raw data are converted into a three dimensional matrix of void fraction, α_{ijk} [7] (where the subscript j, k represent spatial dimensions, and the subscript i indicates the frame number). The total number of frames acquired is simply the total measurement time multiplied by the detector frequency.

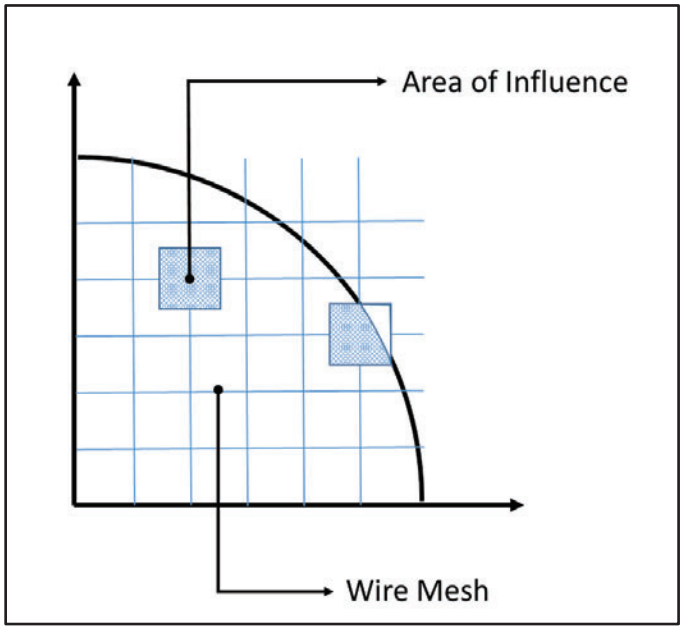

Figure 3: Wire intersections measure local conductivity. Intersections at the edge need to account for a smaller area of influence.

The HZD algorithm uses α_{ijk} as part of its input, together with a bubble identification number b_{ijk}, and a bubble velocity. The matrix b_{ijk} is generated by a recursive algorithm which identifies connected regions of void-fraction (bubbles) [11]. The bubble velocity v_{jk} in the spatial plane of the measurement is estimated using cross-correlation techniques [12]. For the synthetic bubbles, all inputs can be provided exactly.

The HZD algorithm iterates through α_{ijk}, sweeping through j, k then moving to the next frame i. Figure 4 displays the hexahedral domain of analysis for each element in α_{ijk}. In each iteration, the 7 neighboring void fraction values of α_{ijk} are analyzed. Further, four prisms are formed, each containing four void fraction values (one such prism is displayed inside the cube, in Figure 4).

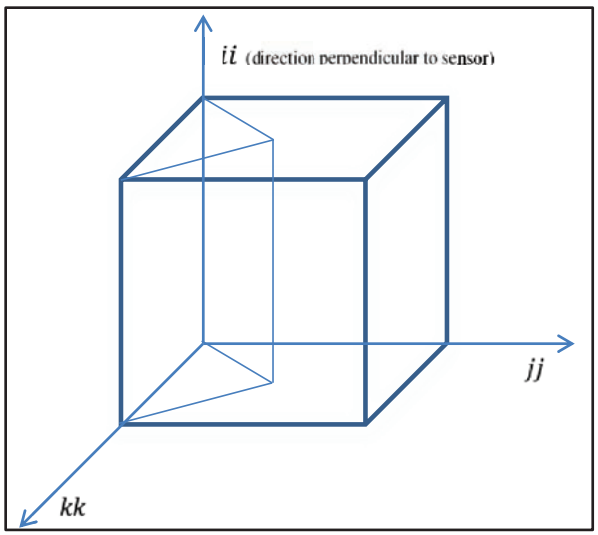

Figure 4: A hexahedral domain about a void fraction point under analysis; the spatial dimensions are indicated by axis kk and jj, temporal dimension is indicated by axis ii.

The top and bottom horizontal planes of the prism are analyzed separately. This results in analysis of two triangles, as displayed in Figure 5. The exterior void fraction points are taken from α_{ijk} (located at the corners of the prism) while the internal void fraction point is an average of the four i-th void fraction points (located at the corners of the i-th horizontal hexahedral plane). Using linear interpolation, the coordinates of the liquid-gas interface are determined.

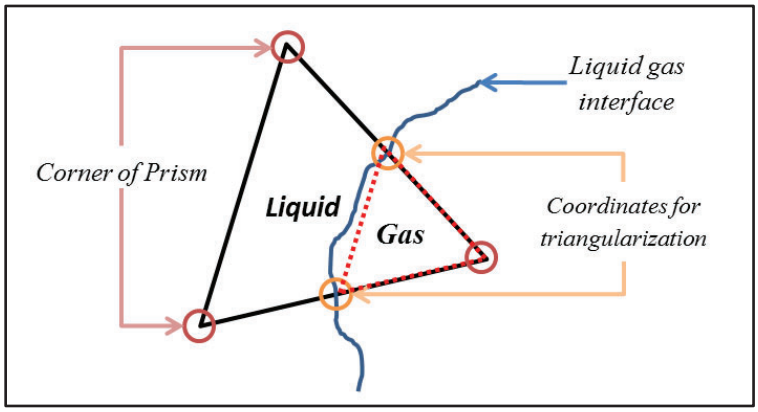

Figure 5: Detection of liquid-gas interface at the horizontal faces of prisms formed within the hexahedral domain.

Once the top and bottom coordinates of the liquid-gas interface are known, a skew quadrilateral can be formed, as displayed in Figure 6. The area of the quadrilateral is estimated by summing the area of 20 triangles. The next three prisms within the hexahedral domain of analysis are analyzed with the same procedure. The algorithm accounts for the absence of a liquid-gas interface.

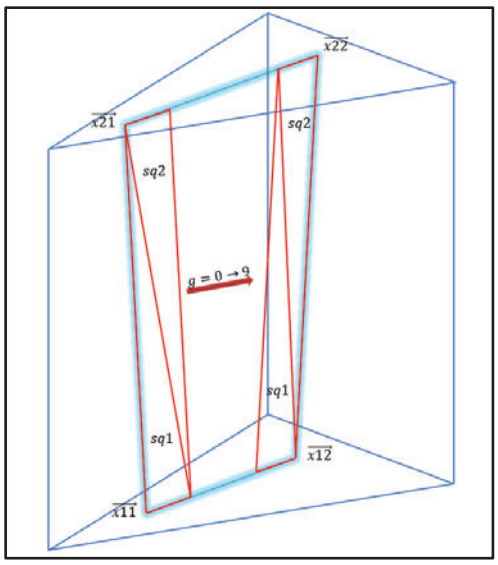

Figure 6: Triangularization of a skew quadrilateral in order to determine the area of the liquid-gas interface.

Once the entire matrix α_{ijk} has been analyzed, the estimated values of the interfacial area of each bubble recorded is available, and therefore the average interfacial area concentration, a_i. In the next section the accuracy of the algorithm is analyzed.

3. UNCERTAINTY ANALYSIS RESULTS

In the following figures, the relative error is determined by Eq. (2).

$$Relative\ error = \frac{a_i^{calculated} - a_i^{actual}}{a_i^{actual}} \times 100 \tag{2}$$

The interfacial area is determined by the HZD algorithm, described in Section 2. Furthermore, a convex hull algorithm from the CGAL library [13] was utilized as an alternative method to the HZD algorithm to estimate the bubble surface area, and therefore the interfacial area concentration, a_i. The performance of the CGAL and HZD algorithms is presented in the following sections.

3.1 Multiple Spherical Bubbles

A preliminary test consisted of error evaluation for multiple synthetic spherical bubbles. Figure 7 presents results for 1000 bubbles that are randomly distributed in the pipe cross section and randomly sized between 3 and 10 mm. It is assumed that the bubbles move at a velocity of 1 m/s and that the acquisition frequency of the WMS is 2500 Hz. A visual of the synthetic bubbles generated for this case are displayed on the right hand side of Figure 7. The x-axis of the graph in Figure 7 indicates the amount of white noise that is artificially added. The noise perturbs the void fraction distribution by a percentage about its nominal value. The results indicate that with no noise added, there is very little error introduced by the HZD algorithm. Typical WMS noise level on the void fraction measurement is about 2%, for which the HZD surface integration algorithm provides very accurate results (even at 5% noise added, the error remains below 2%). The CGAL algorithm slightly underestimates the interfacial area concentration. Figure 8 presents results for larger number of bubbles generated. As the number of frames is kept constant

(and thus the total flow volume), this represents a tighter packing of bubbles. The magnitude of error remains the same. The CGAL algorithm consistently underestimates the bubbles surface area for the typical experimental noise values of about 2%.

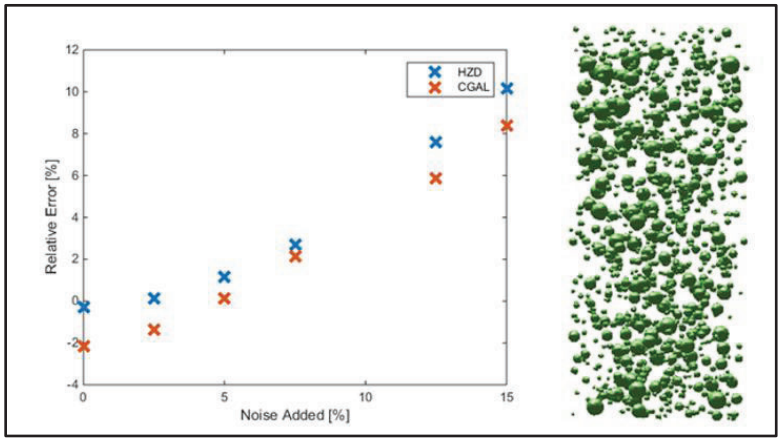

Figure 7: Error on interfacial area concentration for a set of 1000 Spherical bubbles ranging between 3 and 10 mm in diameter, with velocity of 1 m/s.

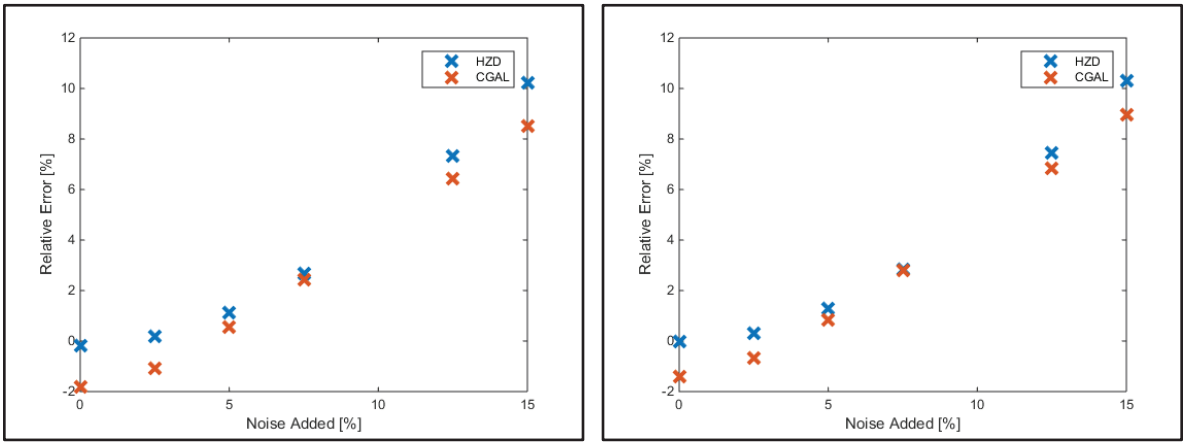

Figure 8: Error for 2000 (left) and 4000 (right) Spherical bubbles between 3 and 10mm at 1 m/s.

3.2 Data Acquisition Frequency

WMS data can be acquired at frequencies, up to 10,000 Hz. Clearly, the higher the acquisition frequency the higher the number of frames available to estimate a given bubble surface. This is illustrated in Figure 9 (the dashed red lines indicate a frame captured by the wire mesh sensor).

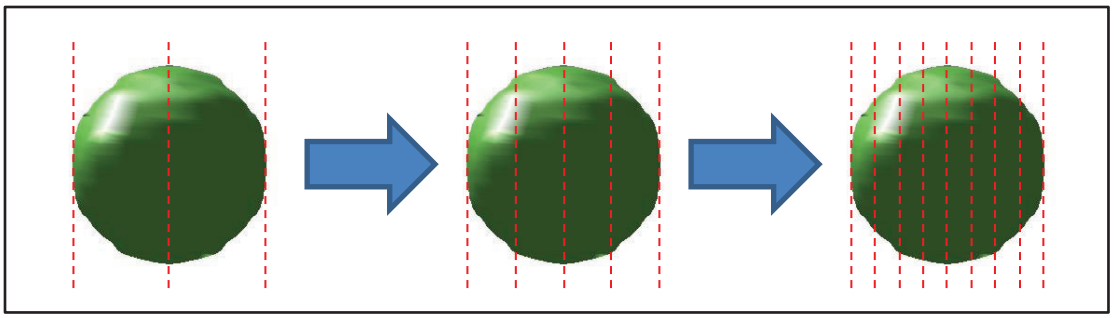

Figure 9: Illustration of the impact of increasing operating frequency on capturing data.

Figure 10 and Figure 11 presents the error in reconstructing the interfacial area as the operating frequency is manipulated for a spherical bubble of 3 mm, 5 mm and 10 mm diameter respectively. The x-axis indicates the bubble displacement that occurs between frames of measurement (this is determined by dividing the bubble velocity by the operating frequency. The higher the acquisition frequency, the lower the displacement of the bubbles between successive frames). In order to concurrently present error introduced by bubble location on the wire-mesh grid, 350 bubbles of equivalent size are randomly distributed in the pipe cross section. The error bars indicate one standard deviation of the error distribution about the mean.

The error on the interfacial area introduced by the HZD algorithm increases slightly for frequencies above 2.5 kHz (below a displacement of 0.4 mm). At high frequencies there is a larger spread in the error due to varying bubble locations. This result indicates that operating at a high frequency is not necessarily beneficial. A similar result is noted for the 5 mm bubble. The 10 mm spherical bubble benefits from its larger size and has a lower error at low operating frequencies. On the other hand, the 10 mm bubble experiences significantly larger error at high operating frequencies (displacement below 0.4 mm). In all cases, the CGAL performs poorer than the HZD algorithm.

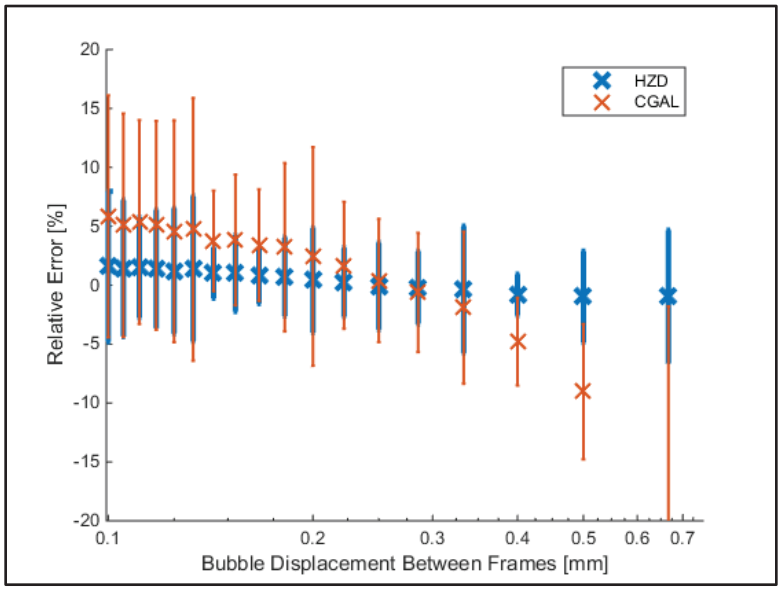

Figure 10: Error for varying operating frequencies for a 3 mm spherical bubble at 1 m/s.

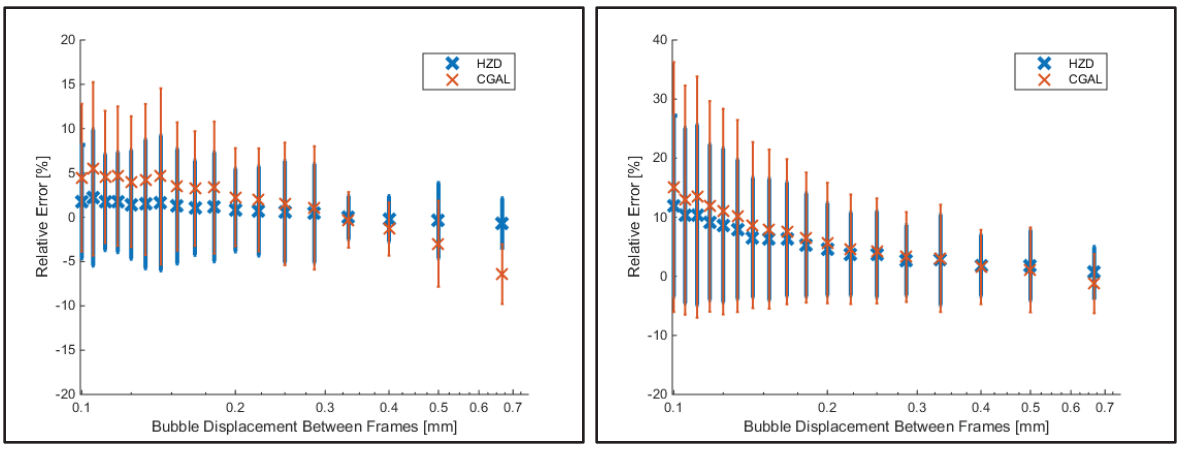

Figure 11: Error for varying operating frequencies for a 5 mm (left) and 10 mm (right) spherical bubble at 1 m/s.

The results presented above indicate that operating at a frequency above 2.5 kHz is not beneficial and rather exacerbates the error introduced by the reconstruction algorithm. Coupled by the fact that the error nearly monotonically increases with increasing frequency (decreasing displacement between frames), it can be asserted that high frequencies can yield a distorted image of the bubble and introduce an overestimation of the surface area. On the opposite end, a similar effect is noted, whereby low frequencies introduce an underestimation of the area.

It is important to note that in general, the optimal operating frequency depends on the bubble size and bubble velocity. Figure 12 presents the error for bubble of various sizes moving at a velocity of 1 m/s, assuming an acquisition frequency of 2.5 kHz. The error for the HZD algorithm is low for 2.5 mm to 7.5 mm bubbles. However, error begins to increase for larger bubbles. For more complicated structures in two phase flow, it would be important to consider the average radius of curvature.

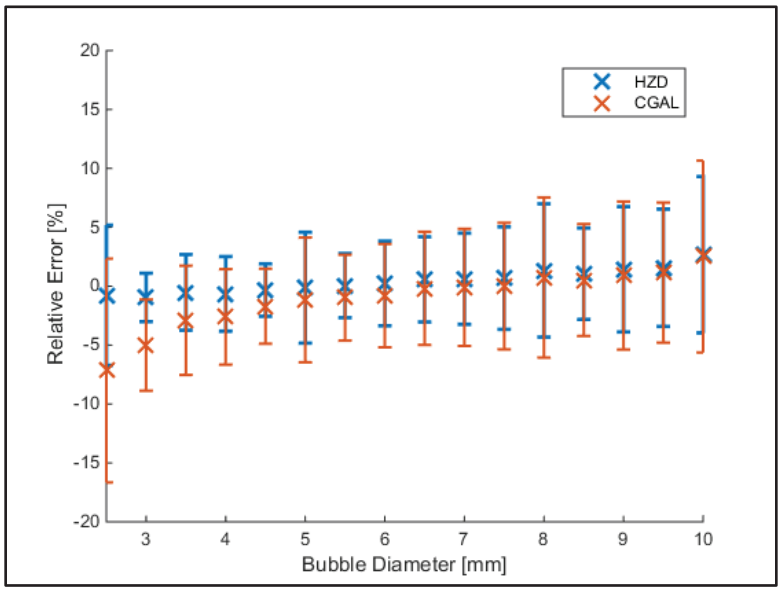

Figure 12: Error for varying bubble diameter at a constant operating frequency of 2.5 kHz (0.4 mm bubble displacement between frames), at 1 m/s.

3.3 Ideal Bullet Bubble

In addition to spherical bubbles, a bullet shaped bubble was also tested. The shape is designed to have a hemispherical head and a cylindrical tail. The length of the tail is modified in multiples of the radius. The results for this shape are presented in Figure 13. The HZD algorithm performs well, decreasing in error as the length of the tail increases. This indicates that the HZD algorithm calculates objects with a simple curvature (such as a cylinder) more accurately, and thus a majority of the error originates from surface area reconstruction of the hemispherical head. The CGAL algorithm is mostly outperformed, but however has a consistent error.

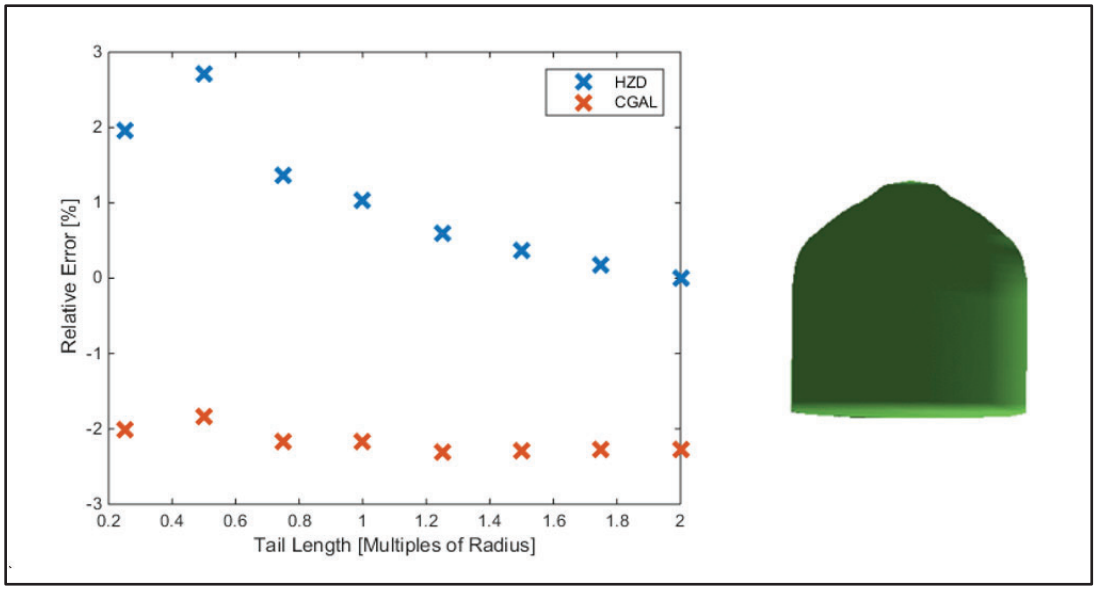

Figure 13: Error for a 10 mm ideal bullet shaped bubble with varying tail lengths at 1 m/s.

3.4 Ideal Bullet Bubble with Internal Cavity

In order to complicate the geometry of the bullet bubble, an internal cavity at the tail end was introduced. The internal cavity is assumed to have the same geometry as the head, i.e. hemispherical. The right hand side of Figure 14 provides a visualization of the bubble's vertical cross-section. It was expected that since the algorithm handles the hemispherical head of the bullet bubble, it would be capable of addressing the internal cavity. However, as indicated by the magnitude of errors in Figure 14, both algorithms tested have been unsuccessful.

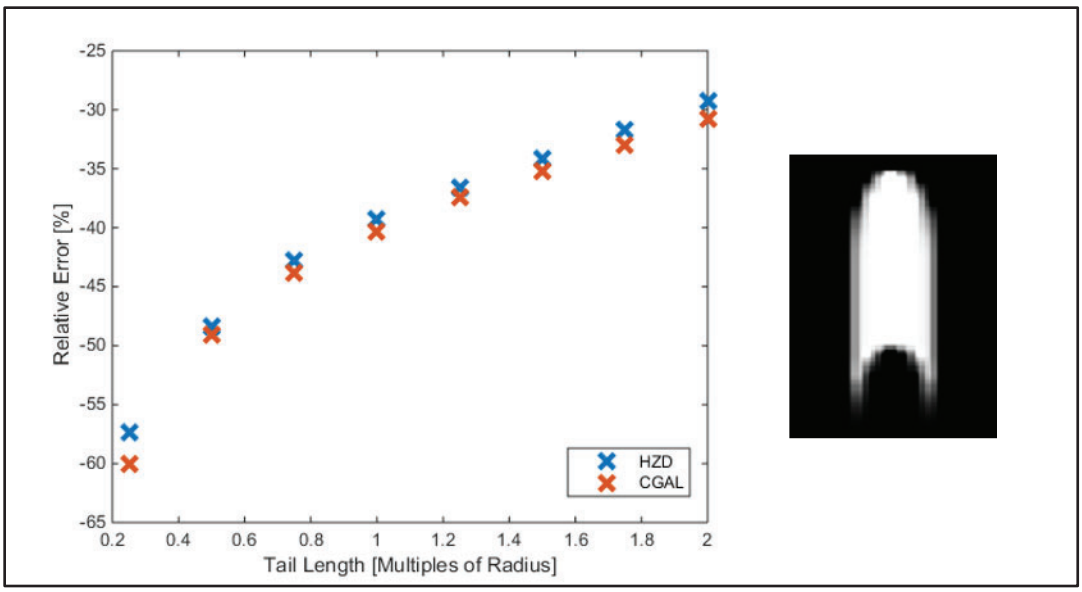

Figure 14: Error for a 10 mm ideal bullet shaped bubble with an internal cavity and varying tail lengths at 1 m/s.

The notion that the internal cavity is introducing a large error can be inferred upon further analysis of Figure 14. As displayed in Figure 13, the ideal bullet bubble without the internal cavity and equivalent specifications has an error less than 3%. Furthermore, as the length of the tail increases (i.e. the proportion of total surface area contribution from the cylindrical body increases) the error decreases. As discussed previously, the algorithms are capable of handling simple cylindrical surfaces. As the CGAL algorithm follows the error propagation of the HZD algorithm, the source of the error stems from the generation of coordinates for triangularization.

Upon debugging the HZD algorithm, it was found that the algorithm ignored void fraction values that comprised the 'skirt' of the bubble. Figure 15 presents visualizations of three frames that comprise the bubble. The actual edges of the bubble are presented by continuous lines (blue indicating an outer edge, red indicating an inner cavity edge). The coordinates that are generated by the HZD algorithm for interfacial area reconstruction are also presented (red crosses). At frame 6, the coordinates successfully wrap around the hemispherical head of the bubble. At frame 16, coordinates are successfully generated for the outer and inner edge, though with less accuracy for the inner edge. However, at frame 20, no coordinates are generated. This occurs because the code is designed to overlook isolated low void fraction values in the 2D void fraction matrix. Further research in this problem is currently being carried out, as similar cavities are present in more complicated bubble structures.

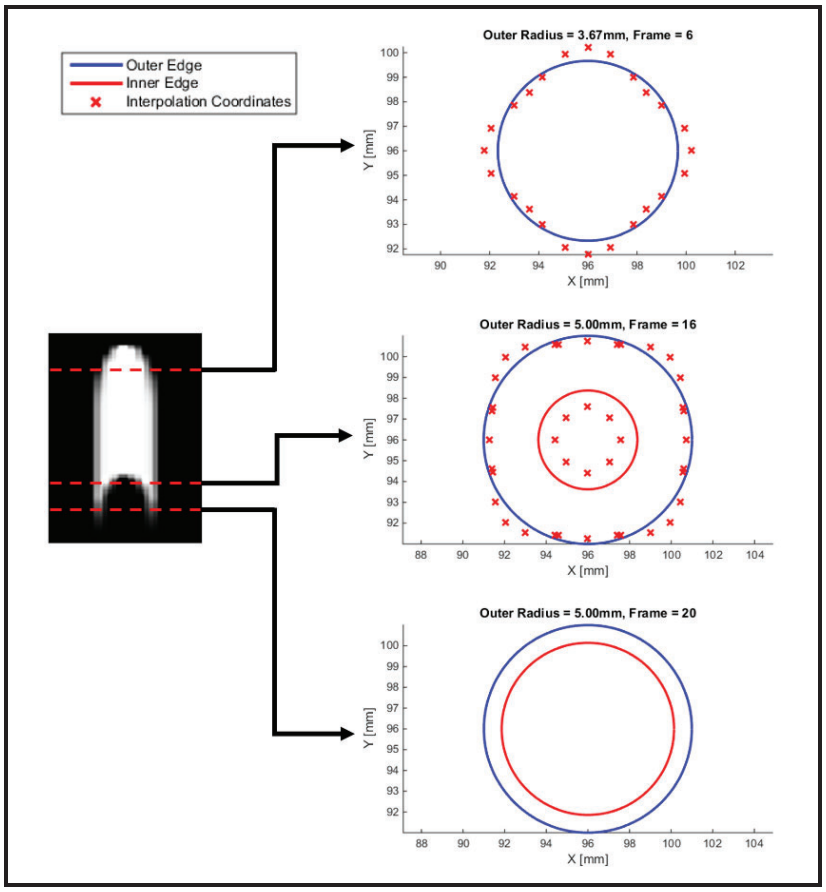

Figure 15: Three separate frames during the computational analysis of the bullet bubble with cavity. The continuous lines indicate the synthetic shape's inner and outer edge. Discrete data represent points that have been interpolated by the HZD algorithm.

3.5 Bubbles Approaching Coalescence

In typical two-phase flows, bubbles are subject to break-up and coalescence. In this section we analyze the accuracy of the interfacial area reconstruction algorithm when two bubbles are merged together. Two spherical bubbles are modeled, one of 15 mm and the other of 20 mm. The process of coalescence is visualized in Figure 16. The primary objective for this case is to determine if the HZD algorithm is capable of calculating the area of a complex shape. Figure 17 presents the error for this case, where the x-axis represents the normalized distance between the centroids of the bubbles. As experienced with the ideal bullet bubble, it is expected that the error will be greatest when the shape being analyzed is complex – this would occur at the onset of coalescence. The propagation of the error supports this expectation. However, the error remains low for all configurations. The CGAL algorithm performs better than the HZD algorithm for this case.

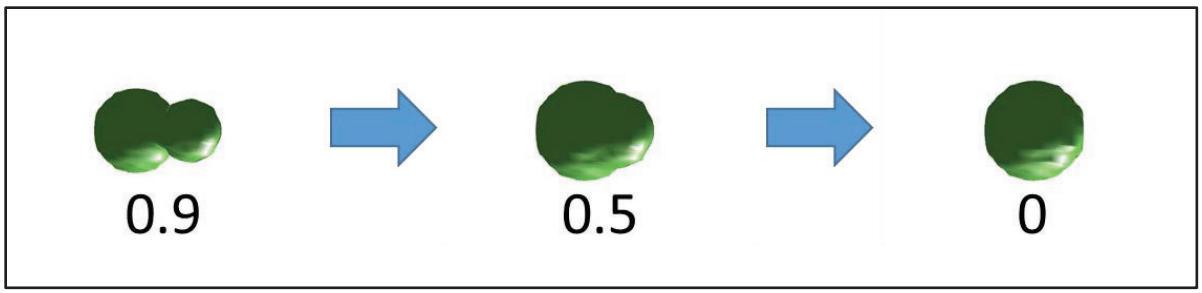

Figure 16: Visual of a 15 mm bubble coalescing into a 20 mm bubble traveling vertically at 1 m/s. The numeric values indicate the normalized proximity of the bubble centroids.

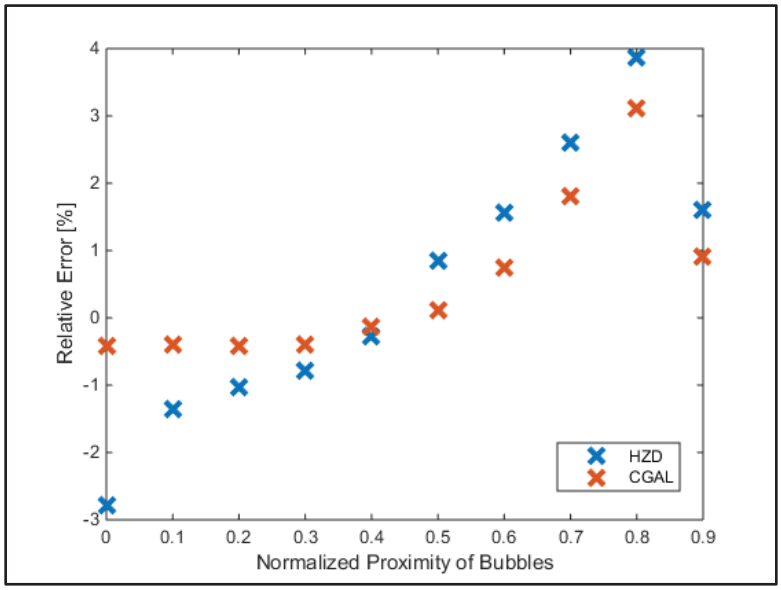

Figure 17: Error for an ideal bullet shaped bubble with varying tail lengths.

4. CONCLUSIONS

Several studies have focused on the validation of the IATE model. For a comprehensive database for two-phase flow experiments, the churn-turbulent and annular flow regime must be studied. Wire mesh sensors have provided an avenue for studying these complex regimes. Before any meaningful validation of the IATE model using the wire mesh sensor data, it is necessary to verify the algorithms used to extract interfacial area and assess their accuracy. The focus of this study is to provide quantitative estimations for the error that is introduced by the interfacial area reconstruction algorithms.

While a majority of the cases have indicated that the error introduced is low (generally less than 5%), it is imperative to note that actual bubble shapes can deviate significantly from the ideal spherical shape. The idealized bullet bubble with an internal cavity exposed issues with the HZD algorithm. This study has indicated that while the algorithm successfully analyzes convex shapes, detection of concave shapes needs improvement. Addressing the issue of successfully analyzing concave shapes is the focus of future research efforts.

ACKNOWLEDGMENTS

The work presented utilizes code provided by Helmholtz-Zentrum Dresden-Rossendorf and has been partially sponsored by the United States Nuclear Regulatory Commission, grant No. NRC-HQ-60-14-G-0008.

REFERENCES

1. M. Beyer, D. Lucas, J. Kussin, P. Schütz, "Air-water experiments in a vertical DN200-pipe," *Forschungszentrum Dresden Rossendorf* (2008).
2. M. Ishii, T. Hibiki, "Thermo-fluid dynamics of two-phase flow 2nd Edition," *Springer*, New York (2010).
3. M. Ishii and S. Kim, "Development of One-group and Two-group Interfacial Area Transport Equation," *Nucl. Sci. Eng.* **146**(3), pp. 257-273 (2004).
4. J. Talley, "Interfacial area transport equation for vertical and horizontal bubbly flows and its application to the trace code," *Ph.D. Thesis, Pennsylvania State University* (2012).
5. M. Bernard, T. Worosz, S. Kim, C. Hoxie, S. Bajorek , "Comparison of Results in the Prediction of Cap/slug flows between Trace-T and Trace V5.0 Patch 3," *NURETH-15* (2013).
6. T.R. Smith, J. P. Schlegel, T. Hibiki, and M. Ishii, "Two-phase flow structure in large diameter pipes," *International Journal of Heat and Fluid Flow*, **Vol. 33**, (2012).
7. H.-M. Prasser, A. Bottger, and J. Zschau, "A new electrode mesh tomograph for gas-liquid flows," *Flow Measurement and Instrumentation*, **9**, pp. 111-119 (1998).
8. Euh, D.J., B.J. Yun, C.H. Song, T.S. Kwon, M.K. Chung, and U.C. Lee, "Development of the five-sensor conductivity probe method for the measurement of the interfacial area concentration." *Nuclear Engineering and Design*, **205**, pp. 35-51 (2001).
9. A, Manera, B. Ozar, S. Paranjape, M. Ishii, and H. Prasser, "Comparison between wire-mesh sensors and conductive needle-probes for measurements of two-phase flow parameters." *Nuclear Engineering and Design,* **239**, pp. 1718-1724 (2008).
10. D. Lucas, M. Beyer, "A new database on interfacial area density obtained from wire-mesh sensor measurements," *NURETH-15* (2014).
11. H.-M. Prasser, "Evolution of interfacial area concentration in a vertical air-water flow measured by wire-mesh sensors", *Nuclear Engineering and Design*, **237**, pp. 1608-1617, 2007
12. A. Manera, H.M. Prasser, D. Lucas, T.H.J.J. van der Hagen, "Three-dimensional flow pattern visualization and bubble size distribution in a stationary and transient upward flashing flow", *International Journal of Multiphase Flow*, **32** (8), pp. 996-1016 (2006).
13. CGAL, Computational Geometry Algorithms Library V. 5.4 (2015), http://www.cgal.org